Diagnostics for transport phenomena in strongly coupled dusty plasmas

J Goree, Bin Liu and Yan Feng†

Department of Physics and Astronomy, The University of Iowa, Iowa City, Iowa 52242, USA

Abstract.
Experimental methods are described for determining transport coefficients in a strongly coupled dusty plasma. A dusty plasma is a mixture of electrons, ions, and highly charged microspheres. Due to their large charges, the microspheres are a strongly coupled plasma, and they arrange themselves like atoms in a crystal or liquid. Using a video microscopy diagnostic, with laser illumination and a high speed video camera, the microspheres are imaged. Moment-method image analysis then yields the microspheres' positions and velocities. In one approach, these data in the particle paradigm are converted into the continuum paradigm by binning, yielding hydrodynamic quantities like number density, flow velocity and temperature that are recorded on a grid. To analyze continuum data for two-dimensional laboratory experiments, they are fit to the hydrodynamic equations, yielding the transport coefficients for shear viscosity and thermal conductivity. In another approach, the original particle data can be used to obtain the diffusion and viscosity coefficients, as is discussed in the context of future three-dimensional microgravity experiments.

† Present address: Los Alamos National Laboratory, Mail Stop E526, Los Alamos, New Mexico 87545, USA; yanfengui@gmail.com

1. Introduction

Dusty plasma [1, 2, 3, 4, 5] is a low-temperature mixture of micron-size particles of solid matter, neutral gas atoms, electrons and ions. The solid particles are typically polymer microspheres, and they are referred to as "dust particles." They each gain a large negative charge Q of about -10^4 elementary charges, for a 7 micron sphere in a typical gas-discharge plasma. Most of the volume is filled with electrons, ions and gas, while the solid particles fill a volume fraction less than 10^{-3}. The motion of the dust particles is dominated by electric forces due to the local electric field $\mathbf{E} = \mathbf{E}_{\rm conf} + \mathbf{E}_d$, where $\mathbf{E}_{\rm conf}$ is due to the ambient plasma potential $V_{\rm conf}$, which can levitate and confine the dust particles. The field $\mathbf{E}_d$ is due to Coulomb collisions with other dust particles.

Due to their high charges, Coulomb collisions among dust particles have a dominant effect. The interaction force $Q\mathbf{E}_d$ among them is so strong that the dust particles do not move easily past one another, but instead self-organize and form a structure that is like that of atoms in a solid or liquid [6, 7, 8, 9, 10, 11, 12, 13]. In other words, the collection of dust particles is said to be a strongly coupled plasma [14]. The pressure p in a strongly-coupled plasma is due mainly to $\mathbf{E}_d$, while thermal motion, which dominates for weakly coupled plasmas, contributes less [15].

This paper is based on a presentation at the EPS Satellite Conference on Plasma Diagnostics 2013. Our emphasis is on the diagnostic methods for determining transport coefficients in a strongly coupled dusty plasma. We start by reviewing the spatially and temporally resolved imaging instrumentation that yields precise measurements of the positions of individual particles [16] and velocities [17]. This capability of making measurements in the particle paradigm is unique in the field of plasma physics diagnostics. To illustrate several methods of transport coefficient determination, we summarize how we determine viscosity and thermal conductivity as in our previously reported two-dimensional (2D) laboratory experiment [18, 19] and we discuss the measurement of viscosity and diffusion coefficients in future 3D microgravity experiments.

2. 2D Experiment

To prepare a 2D experiment to determine transport coefficients, dust particles can be levitated in a single layer by the electric field in the sheath above a horizontal lower electrode in an argon capacitively coupled radio-frequency (rf) plasma, figure 1(a). The 13.56 MHz waveform on the lower electrode, as compared to the grounded vacuum chamber, is 214 V peak-to-peak with a dc self-bias of -138 V. Accordingly, the plasma has both rf and dc electric fields; the rf portion serves only to accelerate electrons and sustain the plasma's ionization, while the dc portion provides levitation of the dust particles.

Melamine-formaldehyde (MF) microspheres of 8.09 μm diameter are introduced by agitating a centimeter-size metal "shaker" box with a small opening so that the particles

sediment through the plasma. They become levitated at a height where the downward force of gravity is balanced by a large upward dc force. (Note that this large force is eliminated in microgravity experiments, section 6.) The box is then retracted. Viewing from the side with an analog video camera and laser illumination, we determine whether there is an unwanted second layer of heavier particles, which can consist of two dust particles stuck together. We remove these heavy particles by modulating the rf power so that the plasma is extinguished in cycles, with plasma-off and plasma-on intervals of about 700 and 10 μs, respectively. This modulation alters the dc electric fields so that particles are levitated at a lower height, near the lower electrode, and the heaviest particles actually touch the electrode and stick. This modulation is repeated in bursts of $\approx 10^2$ cycles while viewing video monitors until all the heavy particles are eliminated. Afterwards, the plasma is operated in steady conditions, and the same particles remain confined in a single layer in the plasma during the entire experiment.

The dust particles move more easily within this single horizontal layer than in the vertical direction, due to the strong vertical gradient of the dc electric field in the electrode sheath. Thus, the particle motion is mainly two dimensional. The dust particles repel one another with a shielded potential, due to the screening provided by the ambient electrons and ions [20]. As the dust particles move, they also experience drag with a force that can be modeled using the Epstein formula [21], which is characterized by a gas damping rate $\nu_{\rm gas}$, which is the ratio of the drag force and the particle's momentum. For the 2D experiment described here, the argon pressure is 15.5 mTorr and $\nu_{\rm gas} = 2.7$ s^{-1}.

The diagnostic instrumentation consists of laser illumination and video imaging, figure 1. Dust particles are illuminated by a sheet of laser light, which is made by focussing a 488-nm argon laser beam with a pair of spherical lenses and then dispersing the beam into a horizontal sheet. The dispersing is done with either a scanning mirror or a cylindrical lens. Imaging of the dust particles is performed using a cooled 14-bit digital camera (PCO 1600) fitted with a 105 mm Nikon lens and a bandpass filter that admits light within a 10 nm bandpass centered on the laser's wavelength. The camera is operated at a frame rate of 55 frame/s, and the combination of lens and sensor provide a resolution of 0.039 mm/pixel. The particle spacing in the plane has a lattice constant $b = 0.50$ mm, corresponding to a 2D Wigner-Seitz radius [22] of $a = 0.26$ mm, areal number density $n_0 = 4.7$ mm^{-2}, and mass density $\rho = nm_d = 1.97 \times 10^{-12}$ kg/mm^2.

Laser manipulation [21, 23, 24, 25, 26, 27, 28, 29] is a widely used tool in dusty plasma experiments. The radiation pressure force of a laser can be used to drive a steady flow of dust particles, which is useful for determining transport coefficients. In our transport-coefficient experiment, a pair of 2.28 W 532-nm laser beams is used to drive counter-propagating flows with a shear region between them. They are incident at a 6° downward angle to push particles in the $\pm x$ directions, as shown in figure 1. To generate a wider flow than in previous 2D transport experiments [31, 25], the laser beams are rastered to have a rectangular cross section. This rastering resulted in a Lissajous pattern, with frequencies of $f_x = 123.607$ Hz and $f_y = 200$ Hz that are

chosen high enough to avoid exciting longitudinal or transverse waves at the rastering frequency. This laser manipulation scheme results in a counterpropagating flow pattern aligned in the $\pm x$ directions in the center, where we analyze data. The flow pattern closes outside the region of interest that is analyzed. Having a straight flow in a single direction provides symmetries that greatly ease the analysis, when determining transport coefficients.

3. Image analysis

Measuring particle positions and velocities in a dusty plasma experiment can be done using particle tracking velocimetry (PTV). The measurement starts with a bit-map image representing a single frame of the recorded video. As an example, in figure 2(a) is a portion of single video frame from a 2D dusty plasma experiment different from the one described in section 2. Each bright spot represents a microsphere. A single microsphere fills multiple pixels, due to diffraction, as shown in figure 2(b). It is desirable to make it fill even more pixels, as in figure 2(c), as can be accomplished by defocusing the camera lens while increasing the illumination laser power.

Images have random noise in each pixel. This random noise can arise because of fluctuations in the camera's sensor and its electronics, and it has an average value that we term the "background intensity," I_{bg}.

After recording a bit-map image, we use the moment method algorithm [16] to compute the particle position as

$$\mathbf{X}_{calc} = \frac{\sum\limits_{k} \mathbf{X}_k (I_k - I_{base})}{\sum\limits_{k} (I_k - I_{base})}, \tag{1}$$

where the most important quantities are the position $\mathbf{X}_k$ and intensity I_k of a pixel k. The result of equation (1) is a "center of mass" of the bright spot. When the particle fills more than one pixel, this calculation can yield an estimate of the particle position with sub-pixel accuracy. Because of its computational efficiency, the moment method is suited for analyzing large quantities of data. In the 2D experiment described here, millions of particle-position measurements were made from the video images using this method. There are other variants of this method [30].

There are two sources of error in the particle position $\mathbf{X}_{calc}$. One is the random noise, which is a fluctuation in each value of I_k regardless of what is imaged. The other is called "pixel locking," and it is due to the finite size of a pixel on the sensor and the way that the light intensity pattern from the lens is averaged within a pixel. Pixel locking causes computed particle positions to be located at favored positions such as the center or corner of a pixel. We devised and tested an optimized method of using equation (1) to measure particle positions while reducing pixel locking and controlling the effects of random errors, reported in [16], which we summarize next.

With this algorithm, it is necessary to limit which pixels are included in the analysis; this is done by choosing contiguous pixels that are brighter than a threshold value I_{th},

which we select using an optimized procedure presented in section 6 of [16]. We also record an image without dust, which we call a dark-field image. We denote its intensity in pixel k as $I_{dark\ k}$. In equation (1) we subtract a baseline intensity $I_{base\ k}$, calculated separately for each pixel as $I_{base\ k} = I_{dark\ k} + (I_{th} - I_{bg})$, where I_{bg} is the average of $I_{dark\ k}$ for pixels in the image. The threshold I_{th} is chosen by varying it downward until artifacts of pixel-locking are minimized in a sub-pixel map. Most steps in this analysis can be done with the ImageJ [32] code, and errors of 0.1 pixel or smaller can be attained.

After calculating particle positions using equation (1), we calculate particle velocities by subtracting the positions $\mathbf{X}_{calc}$ of the same particle in two different frames and dividing by the time interval between frames. This requires "threading" or tracking a particle between two consecutive frames. Threading is typically done by searching the second image within a specified radius around the particle's position in the first frame; if this search yields one particle, we assume it is the same one. If it yields no particles, or more than one particle, then the particle is not successfully threaded to the next frame. Threading for just two frames usually poses little problem if the frame rate is high enough. Threading for many more frames, however, is needed for diffusion coefficient measurements, and this cannot be done indefinitely because particles eventually move out of the region of interest, or in the case of 3D experiments they move sideways out of the illuminating laser sheet.

4. From particles to continua

Using experimental measurements of their positions and velocities, the dust particles can be described in a particle paradigm. Dusty plasmas are unique in the field of plasma physics for allowing one to work with experimental data in the particle paradigm. However, one often needs to work in a continuum paradigm, with fluid quantities such as number density, flow velocity and temperature that are recorded as a function of position. It is possible to convert data from the particle paradigm to the continuum paradigm (but not vice versa); this conversion is done by averaging the particle data on a spatial grid.

Starting with the positions and velocities of individual particles as determined by PTV, we convert to continuum data by averaging particle data within spatial regions of finite area, which we call bins. A similar binning process is used for the same purpose in particle-in-cell simulations [33]; here we use it with experimental data. For the experiment described here there are 89 bins, which are narrow rectangles aligned in the y direction, as shown in figure 1(b). In all our calculations of the continua quantities, we weight the particle data using a simple cloud-in-cell algorithm [33]. If a particle is located at distances L_a and L_b from the two nearest bins a and b, the weighting factors for these bins are $L_b/(L_a + L_b)$ and $L_a/(L_a + L_b)$, respectively. This weighting scheme reduces noise when a particle crosses from one bin to another. The experimental conditions described here were steady, so we also average data over time. The bin width was chosen to be a, the Wigner-Seitz radius.

Spatially resolved data for the number density, flow velocity, and kinetic temperature are required to determine the transport coefficients. We obtain the number density profile simply by counting the weighted particles in each bin and dividing by the area of the bin. Multiplying by the particle mass or charge then yields the profile of the mass density ρ or charge density ρ_c of the dust continuum. The flow velocity profile v_x and kinetic temperature $T_{\rm kin}$ are obtained similarly. For the temperature, we use the squared velocity fluctuation. Results for the profiles in our 2D transport-coefficient experiment are shown in figure 3. These profiles will be used in the continuity equations, described below, to obtain the transport coefficients.

We can obtain additional dust particle parameters from the velocity data by calculating autocorrelation functions and then Fourier transforming them. This procedure yields spectra of longitudinal and transverse waves in a lattice [34]. We do this without laser manipulation to obtain a good crystal, which allows fitting a dispersion relation (from a theory for a triangular lattice with a Yukawa potential) to the experimental spectra. For our transport-coefficient experiment, we find the charge $Q/e = -9700$, a 2D dust plasma frequency $\omega_p = 75$ s^{-1}, and the particle spacing $a/\lambda_D = 0.5$ (which is written as a multiple of the screening length).

We now list the continuity equations. For mass and momentum they are

$$\frac{\partial \rho}{\partial t} + \nabla \cdot (\rho \mathbf{v}) = 0 \tag{2}$$

and

$$\begin{aligned} \frac{\partial \mathbf{v}}{\partial t} + \mathbf{v} \cdot \nabla \mathbf{v} = \frac{\rho_c \mathbf{E}_{\rm conf}}{\rho} - \frac{\nabla p}{\rho} + \frac{\eta}{\rho} \nabla^2 \mathbf{v} \\ + \left[\frac{\zeta}{\rho} + \frac{\eta}{3\rho} \right] \nabla (\nabla \cdot \mathbf{v}) \qquad\qquad + \mathbf{f}_{\rm ext}, \end{aligned} \tag{3}$$

respectively. The transport coefficients η and ζ are the shear viscosity and bulk viscosity, respectively, and η/ρ is called the kinematic viscosity. Equation (3) describes the force per unit mass, i.e., acceleration, acting on the dust continuum. The last term in equation (3) is due to forces such as gas friction, laser manipulation, ion drag, and any other forces that are external to the layer of dust particles. The third and fourth terms on the right-hand-side of equation (3) correspond to viscous dissipation, which arises from Coulomb collisions amongst the charged dust particles.

The continuity equation for the internal energy is

$$T \left(\frac{\partial s}{\partial t} + \mathbf{v} \cdot \nabla s \right) = \Phi + \frac{\kappa}{\rho} \nabla^2 T + P_{\rm ext}. \tag{4}$$

Here, T is the thermodynamic temperature of the dust continuum and s is its entropy per unit mass. The second term on the right-hand-side of equation (4) is due to thermal conduction. The transport coefficient κ is the thermal conducitivity. It arises from a temperature gradient. The first term on the right-hand-side of equation (4) is due to viscous heating, and it arises from a velocity shear. The viscous heating term Φ depends on the square of the shear, i.e., the square of the gradient of flow velocity,

and its expression has many terms, although it can be simplified for our transport-coefficient experiment by taking advantage of symmetries. The last term is due to the energy contribution from the same external forces $\mathbf{f}_{\text{ext}}$ as in equation (3).

External forces that contribute momentum and energy include gas friction, laser manipulation, and the electric confining force. The latter is balanced by the pressure inside the body of charged dust, $\rho_c \mathbf{E}_{\text{conf}} = \nabla p$, so that only two forces need to be considered: gas friction and laser manipulation. The gas friction force can be calculated using measured particle velocities and a known drag coefficient. The laser manipulation force could also be computed if the laser intensity were known, but this is not necessary if we analyze data only in the spatial regions outside the laser beams, as we do here.

We can simplify the continuity equations by exploiting the steady conditions $\partial/\partial t = 0$, the one-dimensional symmetry of the flow configuration $\partial/\partial x = 0$ and $\overline{v_y} = 0$, and incompressibility $\nabla \cdot v = 0$ for subsonic flows. Within the spatial region where the laser intensity is zero, the equations become

$$\nabla \rho = 0 \tag{5}$$

$$\frac{\partial^2 \overline{v_x}}{\partial y^2} - \frac{\rho \nu_{\text{gas}}}{\eta} \overline{v_x} = 0 \tag{6}$$

$$\Phi + \frac{\kappa}{\rho} \frac{\partial^2}{\partial y^2} T - 2\nu_{\text{gas}} \overline{\text{KE}}/m_d = 0 \tag{7}$$

where

$$\Phi = \frac{\eta}{\rho} \left(\frac{\partial \overline{v_x}}{\partial y} \right)^2 \tag{8}$$

is the viscous heating term, simplified for the symmetry of the experiment. The term with $\overline{\text{KE}}$, which is the local average particle kinetic energy (including both random and flow motion), represents the energy loss due to gas friction. We will use these equations to fit the experimental profiles. In doing so, we will assume that η and κ are independent of temperature [25, 35].

5. Obtaining the 2D transport coefficients

The momentum and energy equations are written so that their right-hand sides are zero. When we use these equations with an input of experimental data, however, the terms will not sum exactly to zero, but will instead sum to a nonzero residual. In order to calculate the transport coefficients η and κ, we treat them as free parameters and we minimize the squared residuals summed over the bins in the central flow region. Using this fitting method, we obtain both transport coefficients simultaneously.

For our experiment, this method yields the kinematic viscosity $\nu = \eta/\rho = 0.69$ mm^2/s and thermal diffusivity $\kappa/(c\rho) = 8$ mm^2/s. These values are the culmination of the experimental methods described above, starting with video imaging and ending with continuum flow profiles that are fit to the continuity equations. They were

obtained simultaneously, from the same experiment, by analyzing the same central region, corresponding to the middle 19 bins, corresponding to the 19 data points in in the middle of Fig. 3. Each bin has a width a.

We note that viscosity can depend on parameters such as shear rate $\partial v_x/\partial v_y$ and temperature [36] [37]. In our experiment these quantities are not uniform within the analyzed 19-bin central region, which leads us to repeat our analysis of viscosity for smaller portions of the flow. There are limits to the spatial resolution that one can hope to achieve in a nonuniformly sheared flow because viscosity is a hydrodynamic quantity that requires local equilibrium. Thus, differences in viscosity are not physically meaningful if they occur on a scale length as small as a. We divide the central region into three portions, each with seven bins that overlap by one bin. We find the kinematic viscosity is 1.30 mm^2/s in the innermost 7-bin portion where the shear rate and temperature are lowest, and 0.70 and 0.67 mm^2/s in the two bordering 7-bin portions where the temperature and shear rate are higher. Thus, there is a systematic decrease of about 50% that is attributable to an increasing shear rate and temperature. This effect is significant compared to random errors of order 0.03 mm^2/s. The same approach of using smaller portions of an inhomogeneous flow could be used for the thermal diffusivity, not shown here.

In addition to our method based on fitting to hydrodynamic equations, another method [37, 38] of obtaining the viscosity from particle-domain experimental measurements was introduced by Hartmann *et al.* [37]. The Hartmann method does not require fitting. The local viscosity is calculated as the ratio of the local value of the shear stress P_{xy} and the local value of the shear rate $\partial v_x/\partial v_y$. The shear stress is obtained from experimental measurements as the sum of a kinetic term $\sum_i m_i v_{xi} v_{yi}$ and a potential term, and this sum is binned to convert to the continuum paradigm. This method yields a spatially resolved profile for the viscosity, which is well suited for experiments where the shear rate is nonuniform. It has been used to quantify shear thinning to describe how viscosity diminishes with shear rate [37].

6. 3D microgravity experiments

We carried out a Langevin molecular-dynamics simulation of a 3D dusty plasma to assess the feasibility of determining transport coefficients in the PK-4 device [39, 40, 41, 42]. This European Space Agency (ESA) facility, which is expected to be launched to the International Space Station, is shown schematically in figure 4. It produces a dc plasma in a glass tube, and it is equipped with laser illumination and video imaging. Flows can be driven by laser manipulation or ion drag.

Our simulation parameters were modeled on quantities reported by other experimenters. We assume the gas is neon at 50 Pa pressure, while the MF microspheres have a radius of $r_p = 3.43$ μm [41], and a mass $m_p = 2.55\times10^{-13}$ kg calculated for a mass density of 1.51 g cm^{-3}. We assume a number density of dust particles $n_d = 3\times10^4$ cm^{-3}, which corresponds to a three-dimensional Wigner-Seitz radius $a = (3/4\pi n_d)^{1/3} = 0.020$

cm. For a 50 Pa gas pressure, the gas friction constant is $\nu_g = 51$ s^{-1}. We assume a particle charge $Q = 8520\ e$, which we estimated [43] by adjusting the charge of 1490 e as obtained from the figure 7(a) in [42] for a smaller $r_p = 0.6$ μm particle. We assume a plasma density $n_e = 2.4 \times 10^8$ cm^{-3} and electron temperature $T_e = 7.3$ eV, which we estimated for 50 Pa neon, using a fitting formula for PK-4 data [42]. As in [42], we assume that the ion temperature is close to the gas temperature, $T_i \approx T_{gas} \approx 0.03$ eV. We assume $\lambda_D = (\lambda_{De}^{-2} + \lambda_{Di}^{-2})^{-1/2} = 8.3 \times 10^{-3}$ cm, where λ_{De} and λ_{Di} are the electron and ion Debye lengths calculated using T_e and T_i, respectively.

We assess the feasibility of determining the shear viscosity and the diffusion coefficient in an experimental scheme that has no flows of the dust particles. For the shear viscosity, instead of using the hydrodynamic equations as we did above for the 2D experiment, here we consider an alternate approach of using the Green-Kubo relation, which requires as its inputs the positions $\mathbf{r}_i$, velocities $\dot{\mathbf{r}}_i$ of each particle i, and the potential ϕ_{ij} between all particle pairs [44]. The conditions must provide random thermal motion with an absence of macroscopic flow, which is different from the conditions we used above for the 2D experiment. When using experimental data, which do not provide a direct measure of potentials, the potentials must be calculated from the positions by assuming a model such as the Yukawa potential for the interparticle forces [44]. For the diffusion coefficient, we compute a time series of the mean-square displacement, which requires threads for the particle positions, and these threads must be sufficiently long in their time duration. The diffusion measurement is challenged by the problem that in the experiment the threads (i.e., the time series of data for a given particle) have a finite lifetime due to particles drifting out of the plane of illumination.

In our simulation we integrate a Langevin equation of motion for each particle i,

$$m_p \ddot{\mathbf{r}}_i = -\nu_g m_p \dot{\mathbf{r}}_i + \zeta_i(t) - \nabla \sum_j \phi_{ij} - \nabla V_{\text{conf}}. \tag{9}$$

We use $N = 12800$ dust particles that interact with a Yukawa potential

$$\phi(r_{ij}) = \frac{Q^2}{4\pi\varepsilon_0} \frac{\exp^{-r_{ij}/\lambda_D}}{r_{ij}}, \tag{10}$$

while experiencing drag on the gas as well as random forces ζ_i from the gas atoms. The confining potential V_{conf} is flat in the analyzed region. Since a higher kinetic temperature is more challenging for the diagnostic, and the dust kinetic temperature T_{kin} exceeds the gas temperature in an experiment, we elevated T_{kin} by applying a multiplier of to the random force ζ in the Langevin equation. We found that a multiplier of 16.7 yields $T_{\text{kin}} = 8.3$ eV.

For the feasibility of measuring the diffusion coefficient D, we calculated the probability distribution function (PDF) as a histogram of particle displacements during a specified time interval, figure 5. The mean-square displacement (MSD) is calculated as a moment of the PDF for various time intervals, and presented as a time series, figure 6. An MSD curve typically has two portions: at small times the motion is ballistic with MSD $\propto t^2$ while at long times it is diffusive with MSD $\propto t$. The diffusion coefficient

is determined from the long-time portion, so that it is necessary to record data for sufficiently long times. From the simulation data we determined $D = 0.051$ mm^2/s. To assess the experimental feasibility, we also must know the transition between the two regimes, which we determined to be $t\omega_p = 5$ corresponding to $t = 32$ ms for the PK-4 parameters we assumed. To determine the diffusion coefficient, the MSD curve should be at least three times as long as the transition time (and preferably longer), meaning at least 100 ms for the predicted experimental conditions. To attain threads of this length, the minimum thickness of the laser sheet, for tracking a particle that starts in the laser sheet's center, would be 142 μm, for the simulated conditions. This is comparable to the typical laser sheet thickness in an experiment, meaning that this measurement appears to be marginally feasible, for the parameters evaluated here. Another feasibility consideration is the camera's resolution, i.e., the size that is imaged by one pixel. To measure D will require sufficient spatial resolution so that errors in the particle position do not spoil the MSD curve. For $D = 0.051$ mm^2/s, an observation time of 100 ms would require that the errors in the measured displacement should be significantly smaller than $\sqrt{0.0051 \text{ mm}^2} = 71$ μm. For an imaging resolution of ≈ 14 μm, an algorithm providing sub-pixel accuracy as in [16] would be required to attain sufficiently small errors.

To assess the feasibility of measuring the viscosity η in the experiment, we calculate the Green-Kubo integrals, equations (1-3) of [44], which require data for particle positions in all three dimensions. Three dimensional imaging schemes for PTV have been demonstrated using digital holography and multi-camera stereoscopic imaging [30]. Such a scheme could be used in future space-based experiments beyond PK-4. In our test, we use simulation data sampled at finite time intervals corresponding to an adjustable camera frame rate. Performing this test, we found that a camera frame rate of at least 30 s^{-1} would be required for the parameters above, so that the error introduced in the calculation of viscosity, due to the finite frame rate, is smaller than 2%.

This work was supported by NSF and NASA.

References

[1] Melzer A and Goree J 2008 in *Low Temperature Plasmas: Fundamentals, Technologies and Techniques*, 2nd ed., edited by R. Hippler, H. Kersten, M. Schmidt, and K. H. Schoenbach (Weinheim: Wiley-VCH), p 129.
[2] Morfill G E and Ivlev A V 2009 *Rev. Mod. Phys.* **81** 1353
[3] Piel A 2010 *Plasma Physics* (Heidelberg: Springer)
[4] Shukla P K and Mamun A A 2002 *Introduction to Dusty Plasma Physics* (Bristol: Institute of Physics)
[5] Bonitz M, Henning C and Block D 2010 *Rep. Prog. Phys.* **73** 066501
[6] Chu J H and I L 1994 *Phys. Rev. Lett.* **72**, 4009
[7] Thomas H M and Morfill G E 1996 *Nature (London)* **379** 806
[8] Melzer A, Homann A and Piel A 1996 *Phys. Rev. E* **53** 2757
[9] Samsonov D, Zhdanov S K, Quinn R A, Popel S I and Morfill G E 2004 *Phys. Rev. Lett.* **92** 255004
[10] Feng Y, Goree J and Liu B 2008 *Phys. Rev. Lett.* **100** 205007
[11] Sheridan T E 2008 *Phys. Plasmas* **15**, 103702
[12] Feng Y, Goree J and Liu B 2010 *Phys. Rev. Lett.* **105** 025002

[13] Hartmann P, Douglass A, Reyes J C, Matthews L S, Hyde T W, Kovács A and Donkó Z 2010 *Phys. Rev. Lett.* **105**, 115004
[14] Ichimaru S 1982 *Rev. Mod. Phys.* **54** 1017
[15] Flanagan T and Goree J 2010 *Phys. Plasmas* **17** 123702
[16] Feng Y, Goree J and Liu B 2007 *Rev. Sci. Instrum.* **78**, 053704
[17] Feng Y, Goree J and Liu B 2011 *Rev. Sci. Instrum.* **82**, 053707
[18] Feng Y, Goree J and Liu B 2012 *Phys. Rev. Lett.* **109**, 185002
[19] Feng Y, Goree J and Liu B 2012 *Phys. Rev. E* **86**, 056403
[20] Konopka U, Morfill G E and Ratke L 2000 *Phys. Rev. Lett.* **84**, 891
[21] Liu B, Goree J, Nosenko V and Boufendi L 2003 *Phys. Plasmas* **10**, 9
[22] Kalman G J, Hartmann P, Donkó Z and Rosenberg M 2004 *Phys. Rev. Lett.* **92**, 065001
[23] Homann A, Melzer A, Peters S, Madani R and Piel A 1998 *Phys. Lett. A* **242**, 173
[24] Juan W T, Chen M H and I L 2001 *Phys. Rev. E* **64**, 016402
[25] Nosenko V and Goree J 2004 *Phys. Rev. Lett.* **93**, 155004
[26] Wolter M and Melzer A 2005 *Phys. Rev. E* **71** 036414
[27] Nunomura S, Samsonov D, Zhdanov S and Morfill G 2005 *Phys. Rev. Lett.* **95**, 025003
[28] Vaulina O S, Petrov O F, Gavrikov A V, Adamovich X G and Fortov V E 2008 *Phys. Lett. A* **372**, 1096
[29] Fink M A, Thoma M H and Morfill G E 2011 *Micrograv. Sci. Technol.* **23**, 169
[30] Block D and Melzer A 2010 *Springer Series on Atomic, Optical, and Plasma Physics* **59** p 135
[31] Feng Y, Goree J and Liu B 2010 *Phys. Rev. Lett.* **104** 165003
[32] Rasband W S 2006 *computer code ImageJ version 1.34* (Bethesda, Maryland: U. S. National Institutes of Health) http://rsb.info.nih.gov/ij/
[33] Birdsall C K and Langdon A B 1985 *Plasma Physics via Computer Simulation* (New York: McGraw-Hill)
[34] Nunomura S, Goree J, Hu S, Wang X, Bhattacharjee A and Avinash K 2002 *Phys. Rev. Lett.* **89** 035001
[35] Nosenko V, Zhdanov S, Ivlev A V, Morfill G, Goree J and Piel A 2008 *Phys. Rev. Lett.* **100** 025003
[36] Donkó Z, Goree J, Hartmann P and Kutasi K 2006 *Phys. Rev. Lett.* **96**, 145003
[37] Hartmann P, Sándor M C, Kovács A and Donkó Z 2011 *Phys. Rev. E* **84**, 016404
[38] Nosenko V, Ivlev A V, and Morfill G E 2013 *Phys. Rev. E* **87**, 043115.
[39] Usachev A, Zobnin A, Petrov O, Fortov V, Thoma M, Kretschmer M, Ratynskaia S, Quinn R, Hoefner H and Morfill G 2004 *Czech. J. Phys.* **54**, C639
[40] Fortov V, Morfill G, Petrov O, Thoma M, Usachev A, Hoefner H, Zobnin A, Kretschmer M, Ratynskaia S, Fink M, Tarantik K, Gerasimov Y and Esenkov V 2005 *Plasma Phys. Control. Fusion* **47**, B537
[41] Thoma M H, Höfner H, Khrapak S A, Kretschmer M, Quinn R, Ratynskaia S, Morfill G, Usachev A, Zobnin A, Petrov O and Fortov V 2005 *Ukr. J. Phys.* **50**, 179
[42] Khrapak S A, Ratynskaia S, Zobnin A V, Usachev A D, Yaroshenko V V, Thoma M H, Kretschmer M, Höfner H, Morfill G, Petrov O F and Fortov V E 2005 *Phys. Rev. E* **72**, 016406
[43] In this estimation, we have adjusted the charge according to the particle radius, assuming that the charge varies linearly with the radius, although it is possible that the actual scaling at this gas pressure is different from linear due to ion-neutral collisions.
[44] Feng Y, Goree J, Liu B and Cohen E G D 2011 *Phys. Rev. E* **84**, 046412

Figure 1. Sketch of the experimental configuration for determining transport coefficients in a 2D dusty plasma. (a) A single layer of dust is levitated, and it is illuminated by a 488 nm laser sheet and manipulated by 532 nm rastered laser beams. (b) The manipulation laser drives counter-propagating flows, which are straight within the central region of interest that is analyzed. Reprinted from [19].

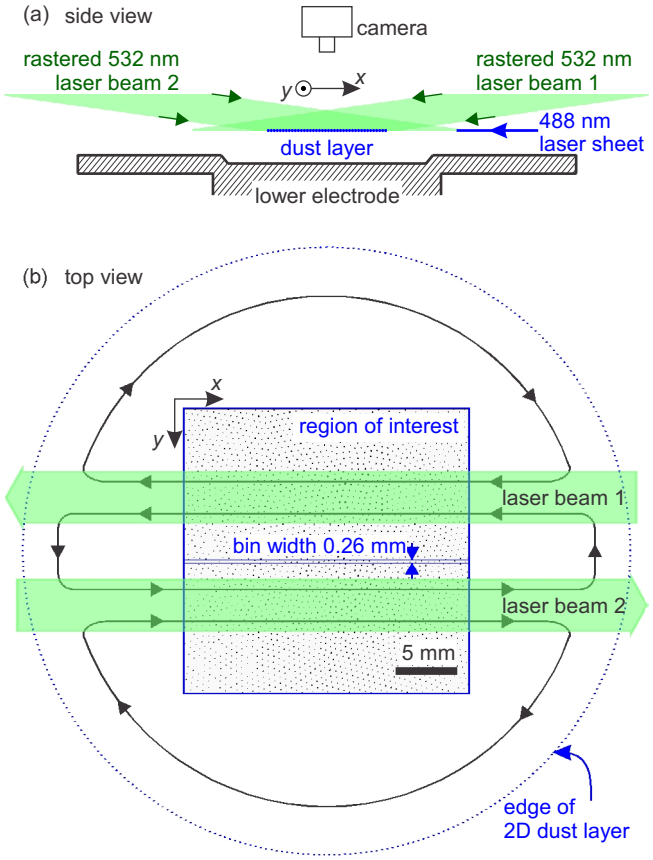

Fig. 1

Figure 2. Bit map images [16]. (a) A 1/12 portion of a bit-map image from an actual experiment, showing the overall crystalline structure in the absence of laser manipulation. (b) and (c) The bright spot for a single particle, from synthetic data. For accurate measurement of position, it is desirable for the random noise seen in each pixel to be minimized, and for the spot to fill many pixels as in (c), with a laser sufficiently powerful to exploit the full dynamic range of the camera's sensor (but without saturating many pixels).

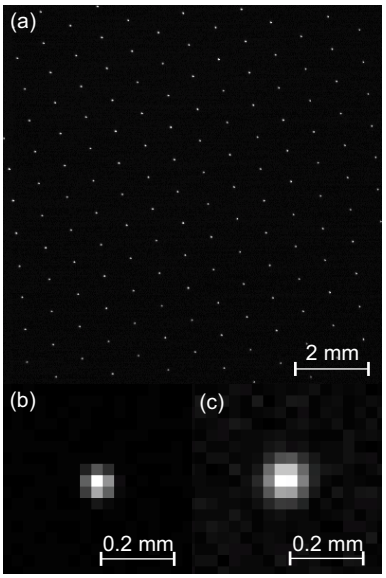

Fig.2

Figure 3. Profiles of the flow velocity (a) and kinetic temperature (b) from the 2D experiment. Fitting these profiles to equations (6-8) yields the transport coefficients for viscosity and thermal conductivity. Note the temperature peaks in the regions of high shear; these peaks are due to viscous heating. Unlike other substances, in a dusty plasma thermal conduction does not overwhelm viscous heating, so that it is possible to detect these viscous heating peaks. Data points correspond to bins of width $a = 0.26$ mm.

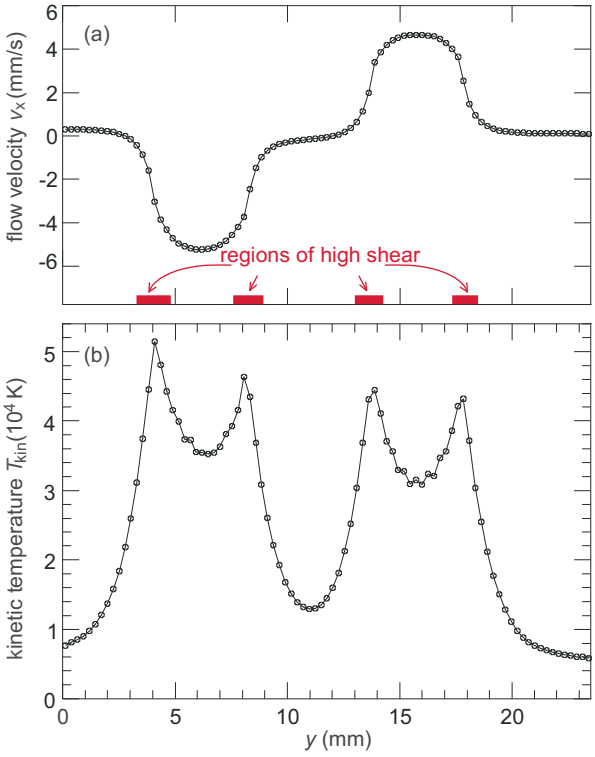

Fig. 3

Figure 4. Sketch of the PK-4 instrument.

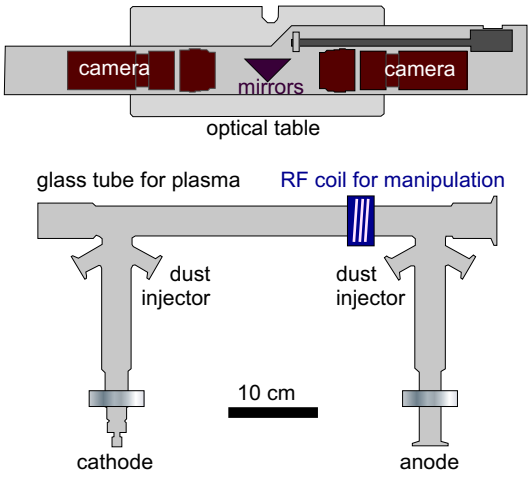

Fig. 4

Figure 5. Probability distribution function (PDF) computed from particle displacements after various times, from our 3D simulation. Time is normalized by the dust plasma frequency ω_p, and displacement is normalized by the Wigner-Seitz radius a.

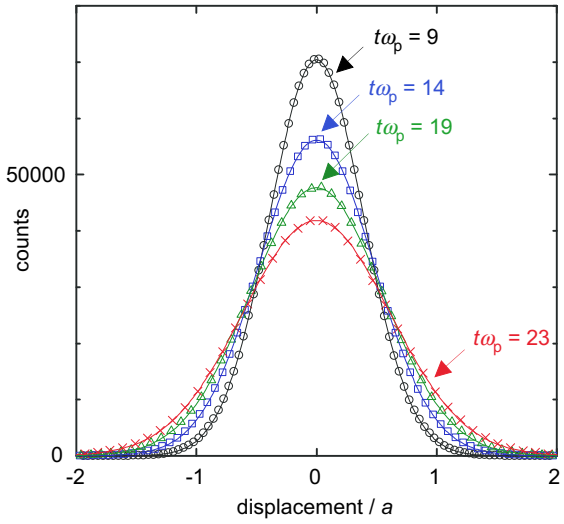

Fig. 5

Figure 6. Mean square displacement (MSD) curves computed from PDF data from our 3D simulation. In an experimental measurement of the diffusion coefficient, it would be necessary to track (thread) particles at least three times as long as the transition time.

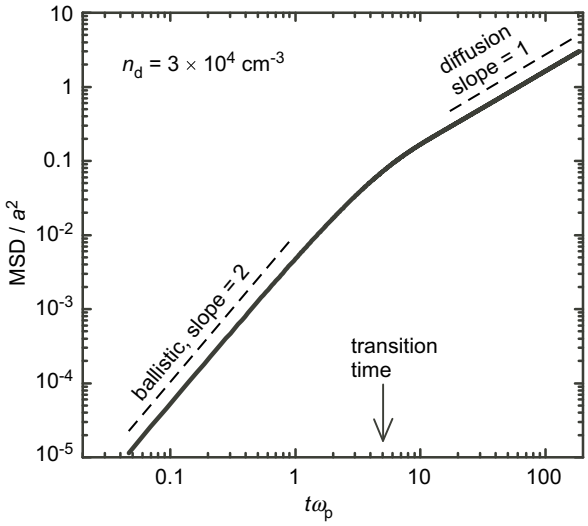

Fig. 6